



CHORUS

This is the accepted manuscript made available via CHORUS. The article has been published as:

Imaging Anomalous Nematic Order and Strain in Optimally Doped $\text{BaFe}_{2}(\text{As,P})_{2}$

Eric Thewalt, Ian M. Hayes, James P. Hinton, Arielle Little, Shreyas Patankar, Liang Wu, Toni Helm, Camelia V. Stan, Nobumichi Tamura, James G. Analytis, and Joseph Orenstein

Phys. Rev. Lett. **121**, 027001 — Published 9 July 2018

DOI: [10.1103/PhysRevLett.121.027001](https://doi.org/10.1103/PhysRevLett.121.027001)

Imaging anomalous nematic order and strain in optimally doped $\text{BaFe}_2(\text{As,P})_2$

Eric Thewalt,^{1,2} Ian M. Hayes,^{1,2} James P. Hinton,^{1,2} Arielle Little,^{1,2} Shreyas Patankar,^{1,2} Liang Wu,^{1,2}
Toni Helm,^{1,2} Camelia V. Stan,³ Nobumichi Tamura,³ James G. Analytis,^{1,2} and Joseph Orenstein^{1,2}

¹*Department of Physics, University of California, Berkeley, California 94720*

²*Materials Science Division, Lawrence Berkeley National Laboratory, Berkeley, California 94720*

³*Advanced Light Source, Lawrence Berkeley National Laboratory, Berkeley, California 94720*

(Dated: March 13, 2018)

We present the strain and temperature dependence of an anomalous nematic phase in optimally doped $\text{BaFe}_2(\text{As,P})_2$. Polarized ultrafast optical measurements reveal broken 4-fold rotational symmetry in a temperature range above T_c in which bulk probes do not detect a phase transition. Using ultrafast microscopy, we find that the magnitude and sign of this nematicity vary on a 50–100 μm length scale, and the temperature at which it onsets ranges from 40 K near a domain boundary to 60 K deep within a domain. Scanning Laue microdiffraction maps of local strain at room temperature indicate that the nematic order appears most strongly in regions of weak, isotropic strain. These results indicate that nematic order arises in a genuine phase transition rather than by enhancement of local anisotropy by a strong nematic susceptibility. We interpret our results in the context of a proposed surface nematic phase.

Iron-based superconductors [1–3] have been the subject of significant interest largely as a result of evidence for quantum criticality [4–12] accompanied by divergent nematic susceptibility [13–17] in the vicinity of optimal doping. These phenomena have been associated with an enhancement of the superconducting critical temperature T_c [18–20].

Evidence for a quantum critical point (QCP) near optimal doping is particularly strong in $\text{BaFe}_2(\text{As}_{1-x}\text{P}_x)_2$, or P:Ba122, an isoelectronically doped superconductor. At high temperature this material has a tetragonal crystal structure, shown in Fig. 1(a), consisting of layers of Fe ions arranged in a square lattice with a pnictogen ion alternating above and below the center of each plaquette, and Ba ions between the layers. The parent compound BaFe_2As_2 undergoes simultaneous tetragonal-to-orthorhombic and Néel spin-density-wave (SDW) transitions at $T_N \approx 150$ K [21], breaking four-fold rotational (C_4) symmetry. Substitution of As by P [22] and c -axis compression [23] each suppress T_N by reducing the average height of pnictogen ions and widening the Fe $3d$ bands, which destabilizes the SDW order [24]. Bulk probes, including neutron and x-ray scattering, transport, NMR [25], and specific heat [9], indicate that the SDW phase onsets above T_c for P concentration up to, but not above, $x = 0.29$, just below optimal doping ($x = 0.3$).

Despite the evidence from these bulk probes, persistent hints that C_4 symmetry is broken in samples with $x > 0.3$ suggest that there is more to the story. Angle-resolved photoemission (ARPES) [26, 27] and torque magnetometry [28] studies have found evidence of broken C_4 symmetry above the dome of superconductivity persisting above optimal doping in P:Ba122, and optical data suggest similar behavior in $\text{Ba}(\text{Fe,Co})_2\text{As}_2$ [29].

The simplest explanation for this apparent discrepancy is that typical samples are under strain. This strain can

either be frozen in during crystal growth, which we call intrinsic strain, or caused by the crystal mounting and cooling processes, which we call extrinsic strain. Such strain, when coupled with diverging nematic susceptibility near the QCP, would induce nematic order that would strengthen rapidly but smoothly with decreasing temperature. However, the measurements of nematicity at $x > 0.3$ indicate that it tends to have an abrupt onset [26, 27, 29], and our results corroborate this observation.

In this letter we present a study of nematicity in optimally doped P:Ba122, with the aim of resolving the apparent contradiction between implications from different experiments. We map a single region of a P:Ba122 crystal with two local probes of broken C_4 : time-resolved optical pump/probe reflectance, or photomodulation, which enhances weak structure in the reflectance R [30]; and scanning Laue microdiffraction [31], which allows us to explore the link between local strain and the onset and strength of nematicity. Our photomodulation measurements reveal nematic order above T_c , with magnitude, sign, and onset temperature varying on a length scale of 50–100 μm .

Contrary to expectation, we find that the nematic order observed via photomodulation is strongest in regions where uniaxial strain and transverse dilation are weakest. However, the boundaries of domains of nematic order coincide with sharp features in local strain. This suggests that the nematic order develops in a genuine phase transition rather than as a result of local anisotropy amplified by strong nematic susceptibility. Our results are consistent with a surface nematic phase, as has been suggested by calculations incorporating interlayer hopping [32]. The existence of such a phase would relieve the tension between results from bulk and surface probes.

Measurements of photomodulated reflectance, ΔR , were performed using linearly polarized, 100 fs

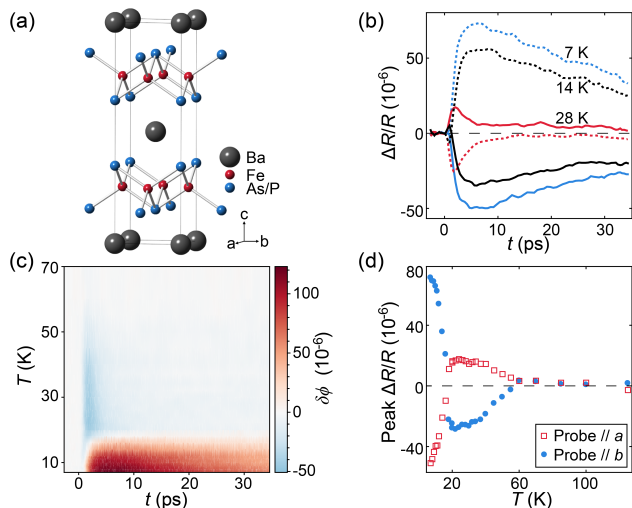


FIG. 1. Crystal structure of P:Ba122 and photomodulation results at optimal doping. (a) Crystal structure of P:Ba122. (b) Pump/probe response $\Delta R/R$ as a function of time at a fixed position, with probe polarization parallel to the Fe–Fe directions a (solid) and b (dotted). Red, black, and blue traces correspond to $T = 28$ K, 14 K, and 7 K, spanning the apparent superconducting transition temperature. (c) Time and temperature dependence of the C_4 -odd photomodulation response $\delta\phi \equiv (\Delta R_b - \Delta R_a)/R$. (d) Temperature dependence of the maximum-amplitude value of $\Delta R(t)/R$ for probe polarization along a (red) and b (blue), illustrating near-perfect antisymmetry under a $\pi/2$ rotation of the probe polarization, abrupt onset of broken C_4 symmetry, and competition between superconductivity and nematic order.

1 duration pulses from a mode-locked Ti:Sapphire laser
 2 at 80 MHz repetition rate, 800 nm center wavelength,
 3 and $\sim 5 \mu\text{J}/\text{cm}^2$ fluence. Our initial measurements
 4 showed strong dependence of the amplitude and sign
 5 of ΔR on the position of the pump/probe focus on the
 6 sample surface. As a result, local characterization of the
 7 time and temperature dependence of ΔR required accu-
 8 rate stabilization of the position of the laser focus relative
 9 to the sample during cooling. This was achieved by reg-
 10 istering the sample to an optical landmark on its mount
 11 using a high-resolution video feed, enabling us to fix the
 12 focal position with a precision of $5 \mu\text{m}$. Figure 1(b) shows
 13 examples of pump/probe traces measured at a fixed po-
 14 sition on a sample with $x = 0.31$ at three temperatures
 15 spanning the apparent superconducting transition, with
 16 the probe polarized along the orthogonal Fe–Fe direc-
 17 tions, which we (arbitrarily) label a and b (solid and dot-
 18 ted, respectively). (The stated temperatures are nomi-
 19 nal; the actual crystal temperature at the laser focus is
 20 higher as a result of laser heating. We studied the appar-
 21 ent superconducting transition temperature as a function
 22 of laser fluence and confirmed that T_c approaches 31 K
 23 at low fluence; the results are shown in [33].)

24 The photomodulation data show striking evidence
 25 of broken C_4 symmetry. In the presence of C_4 81

26 symmetry ΔR would be independent of the polariza-
 27 tion of the probe electric field; that is, $\Delta R_a = \Delta R_b$.
 28 Instead, the pump/probe response is approximately
 29 equal and opposite along orthogonal Fe–Fe directions,
 30 i.e. $\Delta R_a \approx -\Delta R_b$. In subsequent discussion we consider
 31 the strength of the C_4 -odd component of the photomod-
 32 ulation response, $(\Delta R_b - \Delta R_a)/R \equiv \delta\phi$, to be a proxy
 33 for nematic order (see [34] for details).

34 The full time and temperature dependence of $\delta\phi$ is
 35 shown in Fig. 1(c). There are two distinct forms of
 36 pump/probe response: above the superconducting transi-
 37 tion, the response is short-lived and $\delta\phi$ is negative; well
 38 below T_c , the response is long-lived and $\delta\phi$ is positive.
 39 Near the transition, both forms are apparent. To bet-
 40 ter illustrate the singular features of the temperature de-
 41 pendence, we plot in Fig. 1(d) the maximum-amplitude
 42 value of $\Delta R(t)/R$ as a function of temperature for a and b
 43 probe polarizations. With decreasing temperature, ΔR
 44 first appears abruptly above the noise at ~ 60 K. Upon
 45 further cooling, the sign of ΔR changes abruptly near T_c ,
 46 and at low temperature the sign is reversed relative to the
 47 normal state.

48 The change in sign and relaxation rate at T_c can be un-
 49 derstood on the basis of competition between the nematic
 50 order parameter, ϕ , and the superconducting order pa-
 51 rameter, ψ . For $T > T_c$, the pump pulse weakens the
 52 nematic order, which then returns rapidly to its equilibrium
 53 value. However, for $T < T_c$ the pump also suppresses ψ ,
 54 and since the timescale of this suppression is longer than
 55 that of the nematic order a quasiequilibrium results in
 56 which ϕ is enhanced due to the mutual repulsion of ϕ
 57 and ψ . The enhancement of ϕ persists until ψ returns
 58 to its equilibrium amplitude. For a detailed discussion of
 59 this model, refer to [35].

60 The observation of broken C_4 at a fixed location on
 61 the sample surface strongly suggests domain formation as
 62 the origin of the position dependence described above.
 63 To test this hypothesis, we mapped the variation of $\delta\phi$
 64 on the sample surface. These maps were obtained by
 65 mounting samples onto an xyz piezo-stage, and scanning
 66 the sample with respect to an $8 \mu\text{m}$ diameter focus of
 67 overlapping pump and probe beams. The P:Ba122 crys-
 68 tal was mounted on a Cu plate, providing a net 0.2%
 69 compressive strain on the base of the sample via thermal
 70 contraction.

71 A map of local nematicity obtained by spatially re-
 72 solved photomodulation is shown in Fig. 2(a). The
 73 color of each square encodes the maximum-amplitude
 74 value, $\delta\phi_M$, of $(\Delta R_b(t) - \Delta R_a(t))/R$, that is, of the
 75 difference between ΔR measured along the two principal
 76 axes. Domain boundaries separating regions of broken C_4
 77 symmetry with orthogonal nematic order are readily ap-
 78 parent. We note that the typical domain size of $\sim 100 \mu\text{m}$
 79 is large compared to the $\sim 10 \mu\text{m}$ structural domains that
 80 have been imaged using polarized light below the struc-
 81 tural transition in underdoped P:Ba122 [36–38], and that

1 100 μm is the approximate size of crystals used in the pre-
 2 viously cited torque magnetometry experiments that sug-
 3 gested a broad nematic phase above the superconducting
 4 dome [28].

5 The spatial patterns of positive and negative $\delta\phi_M$ do
 6 not change with repeated heating and cooling of the sam-
 7 ple, suggesting that the magnitude and sign of the nem-
 8 atic order are determined by some local quantity. A
 9 local strain field, perhaps frozen into the crystal dur-
 10 ing growth, is a natural candidate; a difference between
 11 the strains along orthogonal Fe–Fe directions would cou-
 12 ple directly to C_4 -breaking order [39]. Another potential
 13 contributing factor is local in-plane compression of the
 14 unit cell [40], which would increase the pnictogen height
 15 and the Fe–As–Fe bond angle, counteracting the effect
 16 of P doping [24] and driving the crystal back toward the
 17 underdoped SDW phase.

18 In order to explore the link between local strain and the
 19 onset of nematic order, we used scanning Laue (i.e., poly-
 20 chromatic) microdiffraction to map the local strain at
 21 room temperature in the same region of the sample that
 22 was imaged using photomodulation (see [41] for details
 23 on the region-alignment procedure). A full diffraction
 24 pattern was collected at each position and used, along
 25 with the known lattice parameters, to extract the deviat-
 26 oric (i.e., traceless) strain tensor ϵ , which describes the
 27 local deformation of the unit cell. In a given basis, the
 28 diagonal components ϵ_{aa} , ϵ_{bb} , and ϵ_{cc} of the strain ten-
 29 sor correspond to expansion (or compression, for negative
 30 values) along the corresponding direction, while the off-
 31 diagonal components ϵ_{ab} , ϵ_{bc} , and ϵ_{ca} correspond to pure
 32 shear. Since we are primarily concerned with strain in the
 33 Fe–As layers, we focus on the ab subsector of ϵ , which
 34 we denote by $\epsilon^{(t)}$. The dilation of the ab -plane unit cell
 35 is given by $\text{Tr } \epsilon^{(t)} = \epsilon_{aa} + \epsilon_{bb}$; compression corresponds
 36 to negative values.

37 Figure 2 illustrates the relationship between the
 38 previously discussed map of low-temperature optical
 39 anisotropy in Fig. 2(a) and the spatial variation of the
 40 strain tensor in Figs. 2(b-d). The superimposed lines,
 41 oriented with the Fe–Fe directions a and b , are posi-
 42 tioned identically on each image. Figure 2(b) shows the
 43 strain anisotropy in the Fe–Fe basis, $\epsilon_{bb} - \epsilon_{aa}$, in the
 44 same region of the crystal. Contrary to what would
 45 be expected if the nematic order were the result of
 46 a local strain bias, the changes in sign of $\delta\phi_M$ and
 47 the Fe–Fe strain anisotropy do not coincide. Further-
 48 more, the Fe–Fe strain anisotropy is small in magni-
 49 tude in most of the region where the nematic photo-
 50 modulation response is strongest. Figure 2(c) shows
 51 the transverse unit-cell dilation $\text{Tr } \epsilon^{(t)}$, which is small
 52 and mostly positive in the large region corresponding
 53 to large positive $\delta\phi_M$, contradicting the prediction that
 54 negative $\text{Tr } \epsilon^{(t)}$ would drive the system toward the
 55 C_4 -breaking SDW phase. Finally, Fig. 2(d) shows the

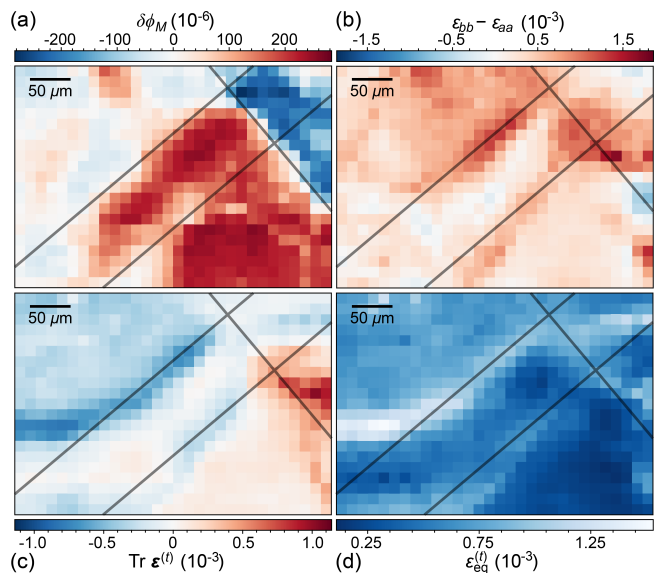


FIG. 2. Spatial variation (13 μm resolution) of optical anisotropy (a) and ab -plane strain (b-d) on a $390 \times 260 \mu\text{m}$ region of an optimally doped P:Ba122 crystal mounted on Cu. (a) Photomodulation proxy for nematic order, $\delta\phi_M$. (b) Transverse strain anisotropy $\epsilon_{bb} - \epsilon_{aa}$ in the Fe–Fe basis. (c) Transverse unit cell dilation $\text{Tr } \epsilon^{(t)}$. (d) Transverse equivalent strain $\epsilon_{\text{eq}}^{(t)} = (2\epsilon_{ij}^{(t)}\epsilon_{ij}^{(t)}/3)^{1/2}$. Superimposed lines are parallel to the Fe–Fe directions and are located at the same positions in each image to facilitate visual comparison of features. Optical data were collected at $T = 5 \text{ K}$; strain data at room temperature.

equivalent strain $\epsilon_{\text{eq}}^{(t)} = (2\epsilon_{ij}^{(t)}\epsilon_{ij}^{(t)}/3)^{1/2}$, a measure of total strain. Although the nematic order and the strain anisotropy are not strongly correlated, the edges of the nematic domains are coincident with strain features; in particular, with local maxima in the equivalent strain and with extrema in $\text{Tr } \epsilon^{(t)}$. (We note that the observed strain variations are likely intrinsic rather than extrinsic, as we observed similar variations in an optimally doped crystal mounted strain-free; see [42] for details.)

Taken together these results strongly suggest that local strain is not the driver, via divergent susceptibility, of the nematicity we observe – in fact, strong strain anisotropy (and strong strain in general) appears to suppress the electronic nematicity.

In order to further study the effect of extrinsic uniaxial strain, we also performed ultrafast microscopy on an optimally doped sample mounted on a piezoelectric stack. On cooling, the piezo provides a tensile uniaxial strain by thermally contracting by 0.1% (similar to optimally doped P:Ba122) along one lateral dimension while expanding by 0.1% along the other. The crystal's Fe–Fe directions were aligned with these principal piezo axes. The resulting image of $\delta\phi_M$ is shown in Fig. 3(a). The domain population of the uniaxially strained crystal differs significantly from that of the Cu-mounted sample,

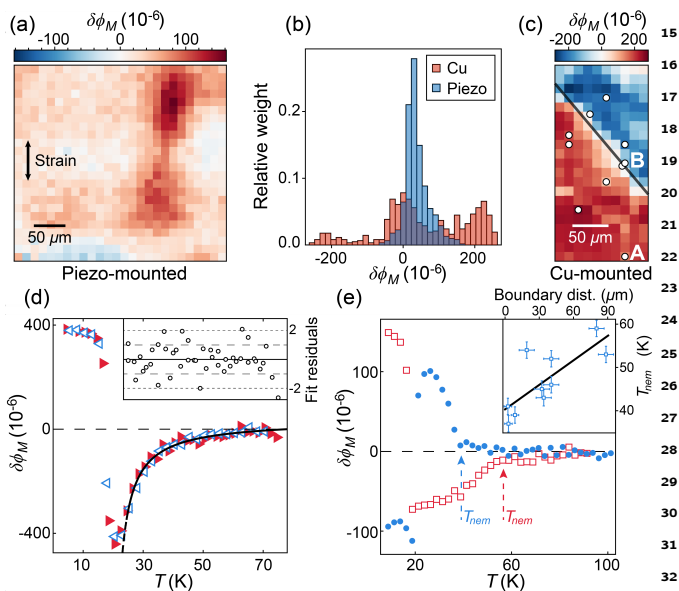


FIG. 3. Comparison of spatial variation (13 μm resolu-
tion) and temperature dependence of nematic order for
piezo-mounted (uniaxially strained) and Cu-mounted (bi-
axially strained) crystals. (a) Spatial variation of photo-
modulation proxy for nematic order, $\delta\phi_M$, on the piezo-
mounted crystal, which is uniaxially strained as indicated.
(b) Histograms showing distribution of $\delta\phi_M$ for both crys-
tals. (c) Spatial variation of $\delta\phi_M$ on the Cu-mounted crys-
tal, with open circles indicating positions at which temper-
ature dependence data was collected and black line marking
a region of null $\Delta R/R$ response separating regions of oppo-
site nematic sign. (d) Temperature dependence of $\delta\phi_M$
for the piezo-mounted crystal while warming (right-pointed
triangles) and cooling (left-pointed triangles). The black
line is a Curie-Weiss fit with $T_{CW} = 19$ K (solid on fitted
domain; dashed at lower temperatures). Inset: standardized
fit residuals. (e) Temperature dependence of $\delta\phi_M$ for the
Cu-mounted crystal far from the boundary at the point marked
A (open squares) and near the boundary at the point marked
B (circles). Apparent nematic transition temperatures are
indicated. Inset: scatter plot of nematic transition tem-
perature and distance from the domain boundary indicated
by the black line in (c); correlation is positive with p -
value $< 10^{-2}$.

1 as is evident in Fig. 3(b), which compares histograms
2 of $\delta\phi_M$ in both samples. The uniaxial strain appears to
3 bias the domain population, shifting the central Cu peak
4 while suppressing the large-amplitude nematic response.
5 Thus, while intrinsic strain defies expectation, extrinsic
6 strain biases the electronic nematicity in the expected
7 manner.

8 In addition to pump-probe microscopy, we measured
9 the temperature dependence of $\delta\phi_M$ on both crystals,
10 including at multiple points on the Cu-mounted sample.
11 These points are indicated by white circles in Fig. 3(c),
12 and the points marked A and B correspond respec-
13 tively to the red and blue $\delta\phi_M(T)$ markers in Fig. 3(e),
14 where $\delta\phi_M$ is plotted as a function of temperature.

The onset of the nematic optical response in the Cu-
mounted crystal is abrupt at each position, and is mani-
festly distinct from a smooth Curie-Weiss behavior. The
onset temperature varies between approximately 40 K
and 60 K and is positively correlated (p -value $< 10^{-2}$)
with distance from the line of null nematic response, as
illustrated in Fig. 3(e). This range of onset tempera-
tures is consistent with ARPES measurements [27] but
is lower than the 100 K onset observed via torque mag-
netometry [28].

In contrast to the Cu-mounted sample, the tempera-
ture dependence of $\delta\phi_M$ on the piezo-mounted crystal
is well-described by a Curie-Weiss form with transition
temperature $T_{CW} = 19$ K. The fit (black line; solid on
fitted region) and data are shown in Fig. 3(d), with the
standardized fit residuals in the inset. In the presence of
strong, uniform uniaxial strain, therefore, we observe a
nematic onset that is consistent with the picture of diver-
gent nematic susceptibility, which makes the sharpness
of the nematic onset in the Cu-mounted sample all the
more notable. We do not observe any hysteretic differ-
ence between the data collected with increasing tempera-
ture (right-pointed markers) and with decreasing tempera-
ture (left-pointed markers).

The strong correlation between the nematic onset tem-
perature and distance from the boundary between the
positive and negative domains suggests that we may be
observing a nucleation phenomenon, where the nematic
domains arise deterministically at some distant crystal-
line features and then spread as the temperature de-
creases until they reach the high-equivalent-strain bound-
aries indicated in Fig. 2(d). This picture is particularly
compelling in light of recent work incorporating hopping
between Fe–As layers, which has shown that interlayer
hopping can produce a surface nematic phase that onsets
at significantly higher temperatures than in the bulk [32].
A surface phase, which could also arise due to stabiliza-
tion of fluctuating order by soft surface phonons [43],
would be more susceptible to confinement by boundaries
of strain due to the reduced dimensionality and volume
of the required region of contiguous deformation, and
could be disfavored under transverse compression due
to buckling-induced disorder. In addition, this model
is consistent both with surface measurements that indi-
cate a genuine nematic phase ([26, 27, 29], this work) and
with bulk measurements that show no evidence of a phase
transition [9, 22, 25]. An important open question that
remains is what mechanism deterministically selects the
sign of the nematic order at a given point on the crystal
surface.

In conclusion, photomodulation measurements reveal
that optimally doped $\text{BaFe}_2(\text{As,P})_2$ has a C_4 -breaking
phase well above T_c that varies strongly in magni-
tude, sign, and onset temperature at length scales
of 50–100 μm . Scanning Laue microdiffraction measure-
ments show that the local strain anisotropy and local

1 transverse compression of the unit cell, which are both 55
 2 expected to favor nematic order, are anticorrelated with 56
 3 the observed optical nematicity. These results imply that 57
 4 the optical nematicity in the biaxially strained crystal 58
 5 corresponds to a genuine nematic phase transition rather 59
 6 than amplification of local anisotropy by enhanced nematic 60
 7 susceptibility. We interpret this phase as a surface 61
 8 phenomenon [32] that nucleates well above T_c and 62
 9 spreads until it reaches boundaries where the crystal is 63
 10 highly strained. A surface nematic phase with large domains 64
 11 reconciles ARPES [26, 27], optical [29], and torque 65
 12 magnetometry [28] measurements showing nematic order 66
 13 at optimal doping with bulk measurements [9, 22, 25] 67
 14 that do not show a phase transition. In general, phase 68
 15 diagrams of two-dimensional materials may differ significantly 69
 16 from those based on bulk measurements of the same 70
 17 compound. 71
 72

18 We thank E. Angelino, R. Fernandes, I. Fisher, F. 74
 19 Flicker, A. Koshelev, K. Song, and N. Yao for helpful 75
 20 discussions. Measurements and modeling were performed 76
 21 at the Lawrence Berkeley National Laboratory in the 77
 22 Quantum Materials program supported by the Director, 78
 23 Office of Science, Office of Basic Energy Sciences, 79
 24 Materials Sciences and Engineering Division, of the U.S. 80
 25 Department of Energy under Contract No. DE-AC02-81
 26 05CH11231. Synthesis of P:Ba122 was supported by Laboratory 82
 27 Directed Research and Development Program of Lawrence 83
 28 Berkeley National Laboratory under Contract No. DE-AC02-84
 29 05CH11231. J.O., L.W., and A.L. received support for performing 85
 30 and analyzing optical measurements from the Gordon and Betty 86
 31 Moore Foundation's EPiQS Initiative through Grant GBMF4537 to 87
 32 J.O. at UC Berkeley. Material synthesis and characterization 88
 33 was supported by the Gordon and Betty Moore Foundation's 89
 34 EPiQS Initiative Grant GBMF4374 to J.A. at UC Berkeley. 90
 35 Laue microdiffraction measurements were carried out at 91
 36 beamline 12.3.2 at the Advanced Light Source. The ALS is 92
 37 supported by the Director, Office of Science, Office of Basic 93
 38 Energy Sciences, of the U.S. Department of Energy under 94
 39 Contract No. DE-AC02-05CH11231. 95
 40 96
 41 97
 98
 99
 100
 101
 102
 103
 104
 105

42 [1] Y. Kamihara, T. Watanabe, M. Hirano, and H. Hosono, 106
 43 *Journal of the American Chemical Society* **130**, 3296 (2008). 107
 44 108
 45 [2] H. Takahashi, K. Igawa, K. Arii, Y. Kamihara, M. Hirano, 109
 46 and H. Hosono, *Nature* **453**, 376 (2008). 110
 47 [3] M. Rotter, M. Tegel, and D. Johrendt, *Physical Review Letters* 111
 48 **101**, 107006 (2008). 112
 49 [4] H. Shishido, A. F. Bangura, A. I. Coldea, S. Tonegawa, 113
 50 K. Hashimoto, S. Kasahara, P. M. C. Rourke, H. Ikeda, 114
 51 T. Terashima, R. Settai, *et al.*, *Physical Review Letters* 115
 52 **104**, 057008 (2010). 116
 53 [5] S. Kasahara, T. Shibauchi, K. Hashimoto, K. Ikeda, 117
 54 S. Tonegawa, R. Okazaki, H. Shishido, H. Ikeda, 118

H. Takeya, K. Hirata, *et al.*, *Physical Review B* **81**, 184519 (2010).
 [6] Y. Nakai, T. Iye, S. Kitagawa, K. Ishida, H. Ikeda, S. Kasahara, H. Shishido, T. Shibauchi, Y. Matsuda, and T. Terashima, *Physical Review Letters* **105**, 107003 (2010).
 [7] E. Abrahams and Q. Si, *Journal of physics: Condensed matter* **23**, 223201 (2011).
 [8] K. Hashimoto, K. Cho, T. Shibauchi, S. Kasahara, Y. Mizukami, R. Katsumata, Y. Tsuruhara, T. Terashima, H. Ikeda, M. A. Tanatar, *et al.*, *Science* **336**, 1554 (2012).
 [9] P. Walmsley, C. Putzke, L. Malone, I. Guillaumon, D. Vignolles, C. Proust, S. Badoux, A. I. Coldea, M. Watson, S. Kasahara, *et al.*, *Physical Review Letters* **110**, 257002 (2013).
 [10] J. G. Analytis, H. H. Kuo, R. D. McDonald, M. Wartenbe, P. M. C. Rourke, N. E. Hussey, and I. R. Fisher, *Nature Physics* **10**, 194 (2014).
 [11] T. Shibauchi, A. Carrington, and Y. Matsuda, *Annu. Rev. Condens. Matter Phys.* **5**, 113 (2014).
 [12] H.-H. Kuo, J.-H. Chu, J. C. Palmstrom, S. A. Kivelson, and I. R. Fisher, *Science* **352**, 958 (2016).
 [13] L. W. Harriger, H. Q. Luo, M. S. Liu, C. Frost, J. P. Hu, M. R. Norman, and P. Dai, *Physical Review B* **84**, 054544 (2011).
 [14] M. Yi, D. Lu, J.-H. Chu, J. G. Analytis, A. P. Sorini, A. F. Kemper, B. Moritz, S.-K. Mo, R. G. Moore, M. Hashimoto, *et al.*, *Proceedings of the National Academy of Sciences* **108**, 6878 (2011).
 [15] J.-H. Chu, H.-H. Kuo, J. G. Analytis, and I. R. Fisher, *Science* **337**, 710 (2012).
 [16] A. E. Böhrer, P. Burger, F. Hardy, T. Wolf, P. Schweiss, R. Fromknecht, M. Reinecker, W. Schranz, and C. Meingast, *Physical Review Letters* **112**, 047001 (2014).
 [17] R. M. Fernandes, A. V. Chubukov, and J. Schmalian, *Nature Physics* **10**, 97 (2014).
 [18] M. A. Metlitski, D. F. Mross, S. Sachdev, and T. Senthil, *Physical Review B* **91**, 115111 (2015).
 [19] S. Lederer, Y. Schattner, E. Berg, and S. A. Kivelson, *Physical Review Letters* **114**, 097001 (2015).
 [20] T. A. Maier and D. J. Scalapino, arXiv preprint arXiv:1405.5238 (2014).
 [21] Q. Si, R. Yu, and E. Abrahams, *Nature Reviews Materials* **1**, 16017 (2016).
 [22] J. M. Allred, K. M. Taddei, D. E. Bugaris, S. Avci, D. Y. Chung, H. Claus, C. dela Cruz, M. G. Kanatzidis, S. Rosenkranz, R. Osborn, *et al.*, *Physical Review B* **90**, 104513 (2014).
 [23] W. J. Duncan, O. P. Welzel, C. Harrison, X. F. Wang, X. H. Chen, F. M. Grosche, and P. G. Niklowitz, *Journal of Physics: Condensed Matter* **22**, 052201 (2010).
 [24] M. Rotter, C. Hieke, and D. Johrendt, *Physical Review B* **82**, 014513 (2010).
 [25] D. Hu, X. Lu, W. Zhang, H. Luo, S. Li, P. Wang, G. Chen, F. Han, S. R. Banjara, A. Sapkota, *et al.*, *Physical Review Letters* **114**, 157002 (2015).
 [26] T. Shimojima, T. Sonobe, W. Malaeb, K. Shinada, A. Chainani, S. Shin, T. Yoshida, S. Ideta, A. Fujimori, H. Kumigashira, *et al.*, *Physical Review B* **89**, 045101 (2014).
 [27] T. Sonobe, T. Shimojima, A. Nakamura, M. Nakajima, S. Uchida, K. Kihou, C. Lee, A. Iyo, H. Eisaki, K. Ohgushi, *et al.*, *Scientific Reports* **8**, 2169 (2018).

- 1 [28] S. Kasahara, H. J. Shi, K. Hashimoto, S. Tonegawa, 19
 2 Y. Mizukami, T. Shibauchi, K. Sugimoto, T. Fukuda, 20
 3 T. Terashima, A. H. Nevidomskyy, *et al.*, *Nature* **486**, 21
 4 382 (2012). 22
- 5 [29] L. Stojchevska, T. Mertelj, J.-H. Chu, I. R. Fisher, and 23
 6 D. Mihailovic, *Phys. Rev. B* **86**, 024519 (2012). 24
- 7 [30] M. Cardona, K. L. Shaklee, and F. H. Pollak, *Physical* 25
 8 *Review* **154**, 696 (1967). 26
- 9 [31] N. Tamura, A. A. MacDowell, R. Spolenak, B. C. Valek, 27
 10 J. C. Bravman, W. L. Brown, R. S. Celestre, H. A. Pad- 28
 11 more, B. W. Batterman, and J. R. Patel, *Journal of* 29
 12 *Synchrotron Radiation* **10**, 137 (2003). 30
- 13 [32] K. W. Song and A. E. Koshelev, *Physical Review B* **94**, 31
 14 094509 (2016). 32
- 15 [33] Supplemental Materials, Sec. S1. 33
- 16 [34] Supplemental Materials, Sec. S2. 34
- 17 [35] Supplemental Materials, Sec. S3. 35
- 18 [36] M. A. Tanatar, A. Kreyssig, S. Nandi, N. Ni, S. L. 36
 37 Bud'ko, P. C. Canfield, A. I. Goldman, and R. Prozorov, *Physical Review B* **79**, 180508 (2009).
- [37] M. A. Tanatar, E. C. Blomberg, A. Kreyssig, M. G. Kim, N. Ni, A. Thaler, S. L. Bud'ko, P. C. Canfield, A. I. Goldman, I. I. Mazin, *et al.*, *Physical Review B* **81**, 184508 (2010).
- [38] J.-H. Chu, J. G. Analytis, D. Press, K. De Greve, T. D. Ladd, Y. Yamamoto, and I. R. Fisher, *Physical Review B* **81**, 214502 (2010).
- [39] H.-H. Kuo, J. G. Analytis, J.-H. Chu, R. M. Fernandes, J. Schmalian, and I. R. Fisher, *Physical Review B* **86**, 134507 (2012).
- [40] A. E. Böhmer, A. Sapkota, A. Kreyssig, S. L. Bud'ko, G. Drachuck, S. M. Saunders, A. I. Goldman, and P. C. Canfield, *Physical Review Letters* **118**, 107002 (2017).
- [41] Supplemental Materials: Sec. S4.
- [42] Supplemental Materials, Sec. S5.
- [43] S. E. Brown, E. Fradkin, and S. A. Kivelson, *Physical Review B* **71**, 224512 (2005).